(Received 17 February 2025, Accepted 16 March 2025, Scheduled 5 April 2025)

Low-Loss, High-Rejection UWB Filter with Dual Sharp Notch Characteristics for Wireless Communications

Ming Ming Gao, Han Ci Jiang*, Yun Shu Yang, Xin Yue Zhang, and Ya He

College of Electronics and Information Engineering, Liaoning Technical University, Huludao, Liaoning, China

ABSTRACT: To improve the requirements of stopband rejection in ultra-wideband (UWB) filters, a modified T-shaped resonator is proposed and optimized based on multimode resonator (MMR) theory. The conventional resonator is enhanced by loading open-circuit branches and introducing circular slots to create transmission zeros, while asymmetric coupling lines and a "ram's horn" structure are employed to realize dual trappings at 6.3 GHz and 6.8 GHz. Additionally, a defective ground structure (DGS) is incorporated to further improve the filter's performance. The proposed filter exhibits a passband range of 3.4 GHz to 11.8 GHz, with a minimum insertion loss of -0.2 dB and a return loss greater than 10 dB. The filter demonstrates excellent steepness of the attenuation in the upper and lower stopbands, with trap depths of -28.4 dB and -50 dB at the trapped frequencies of 6.3 GHz and 6.8 GHz, respectively.

1. INTRODUCTION

Ultra-wideband (UWB) technology was authorized for commercial use by the Federal Communications Commission (FCC) in 2002, and since then, UWB systems have garnered significant attention due to their considerable potential for development in various applications. As a key component of wireless communication systems, the performance of filters — particularly their key parameters — directly influences the overall efficiency and performance of the communication transceiver system. Filters with high out-of-band rejection and low insertion loss are essential for ensuring the optimal operation of these systems. Consequently, the design and optimization of such filters have become a major area of research for experts and scholars [1].

Several studies have proposed various approaches to the design of UWB filters with trapping characteristics. Study [2] introduced a UWB bandpass filter based on an E-type resonator, with open-circuit branches embedded to introduce trapping features. The number of traps can be adjusted by varying the size of the branches. However, the steepness drop coefficient of this design is relatively small, and its out-of-band rejection performance remains suboptimal [3], presenting a UWB filter loaded with step-impedance branches on a conventional dual-mode resonator. While the filter demonstrates excellent passband performance, it suffers from a large lower-blocking band transmission zero, which adversely affects its frequency-selective characteristics. Research [4] proposed a filter design that introduced two hole-backed digital coupling lines on both sides of the resonator. This configuration ensures smooth passband characteristics with low insertion loss. However, due to the absence of trapping mechanisms, the design fails to mitigate interference from other frequency bands within the passband. The authors in [5] designed a filter consisting of parallel resonators with a common feed structure, which exhibits excellent passband performance and deep traps. Nevertheless, the complexity of the structure increases fabrication difficulty, making it less practical for large-scale production.

This paper presents the design of a UWB bandpass filter with dual traps. The design is based on MMR theory, which enables the realization of a UWB response. The proposed filter achieves this by loading four open-circuit branches at both ends of a T-shaped resonator and incorporating a circular slot in a rectangular microstrip line structure at the top. These modifications introduce transmission zeros in both the upper and lower rejection bands, effectively enhancing the filter's selectivity. In addition, two traps are created by bending the input/output parallel coupling lines upwards and adding a "ram's horn" structure at the bottom of the resonator. This design not only provides excellent out-of-band rejection but also mitigates interference from other frequency bands within the passband, addressing a common challenge in filter design [6].

2. ANALYSIS AND DESIGN OF UWB FILTERS

The concept of the MMR was first introduced and applied to the design of compact UWB filters in 2000 [14]. This pioneering approach achieves a fractional bandwidth of approximately 70% by utilizing two distinct resonant modes within the resonator, facilitated by the input and output feed lines.

Building on the principles of multimode resonance theory and transmission line theory, this study proposes a novel resonator structure that improves the conventional T-shaped resonator. The evolution of the proposed design is illustrated in Fig. 1 specifically.

Figure 1(a) depicts the original T-shaped resonator structure. In the next step, the upper end of the resonator is optimized and grooved to enhance performance, as shown in Fig. 1(b).

* Corresponding author: Han Ci Jiang (1511062102@qq.com).

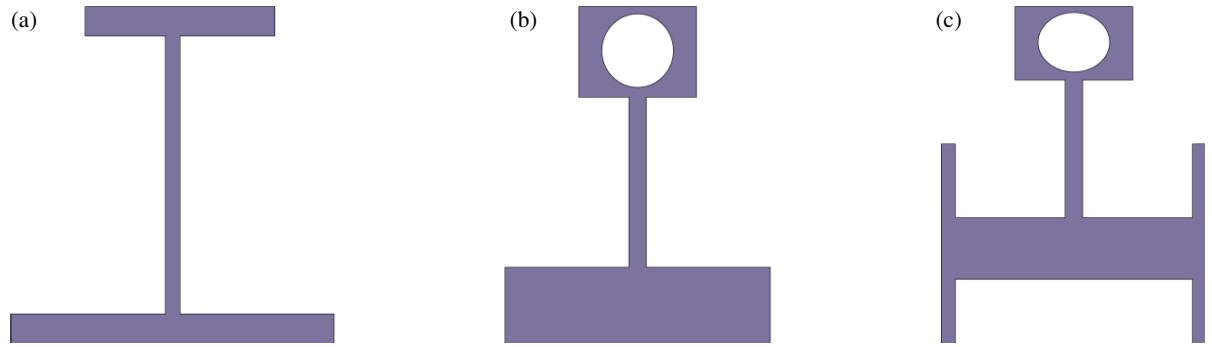

FIGURE 1. New resonator evolution processes. (a) Traditional T-shape. (b) Improvement of trenching treatment. (c) Introducing open branches.

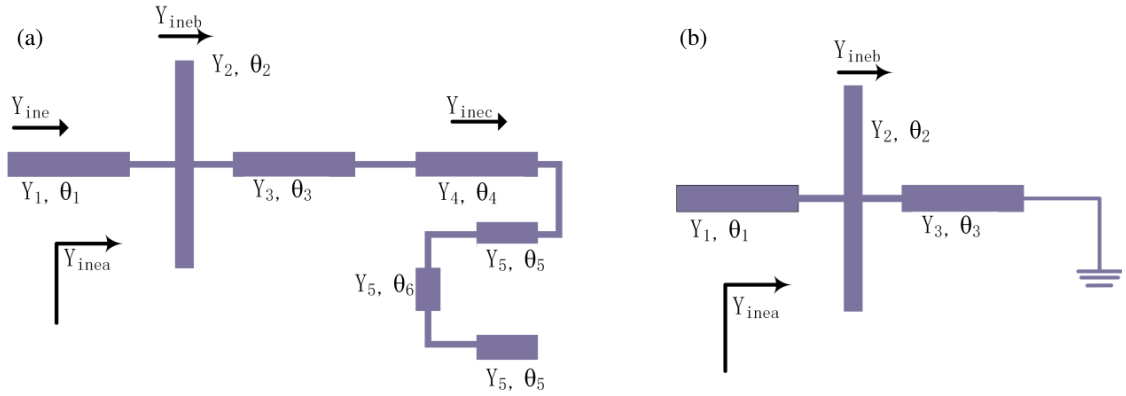

FIGURE 2. Equivalent circuit diagram for parity mode analysis. (a) Coupled-mode equivalent model. (b) Odd-mode equivalent models.

Finally, open-circuit branches are symmetrically loaded at the lower end of the T-shaped resonator, forming the structure illustrated in Fig. 1(c).

The final evolved T-shaped resonator is integrated with a horizontal transmission line to create the new MMR, which exhibits improved performance and broader bandwidth. This innovative design leverages multimode resonance to enable more compact and efficient UWB filter implementations, offering significant advancements over conventional resonator structures.

The proposed MMR is composed of a stepped-impedance transmission line and four symmetrically distributed open-circuit branches. Additionally, the top section of the resonator is loaded with open-circuit stubs, designed in a rectangular shape embedded within a circular structure, to enhance the resonator's performance and mode coupling. The conductance of each branch in the MMR is denoted by Y. The input conductances in various directions are expressed as Y_{inoa}, Y_{Inob}, Y_{inea}, Y_{ineb}, Y_{inec} while the electrical length of each branch is represented by θ.

Due to the symmetric geometry of the modified resonator with respect to the Y-axis, its electromagnetic behavior can be effectively analyzed using the parity-mode symmetry method. This method enables the decomposition of the resonator's response into even- and odd-mode components, simplifying the analysis of its resonant characteristics. The equivalent circuit of the MMR, derived based on parity-mode analysis, is illustrated in Fig. 2. This circuit representation provides a clear framework for understanding the mode coupling and resonance behavior of the proposed structure.

The input conductance of the MMR in Fig. 2(a) at even-mode response is derived from the transmission line theoretical model study:

$$Y_{\text{in,even}} = Y_1 \frac{Y_{\text{inea}} + \text{j}Y_1 \tan\theta_1}{Y_1 + \text{j}Y_{\text{inea}} \tan\theta_1} \tag{1}$$

$$Y_{\text{inea}} = Y_2 \frac{Y_{\text{ineb}} + \text{j}Y_2 \tan\theta_2}{Y_2 + \text{j}Y_{\text{ineb}} \tan\theta_2} \tag{2}$$

$$Y_{\text{ineb}} = Y_3 \frac{Y_{\text{inec}} + \text{j}Y_3 \tan\theta_3}{Y_3 + \text{j}Y_{\text{inec}} \tan\theta_3} \tag{3}$$

$$Y_{\text{inec}} = Y_4 \frac{Y_{\text{ined}} + \text{j}Y_4 \tan\theta_4}{Y_4 + \text{j}Y_{\text{ined}} \tan\theta_4} \tag{4}$$

For the simplicity of calculation, let $\theta_5 = \theta_6 = \theta$, which can be launched:

$$Y_{\text{ined}} = \text{j}Y_5 \frac{3\tan\theta - \tan^3\theta}{1 - 3\tan^2\theta} \tag{5}$$

The equivalent structure of the resonator at odd-mode excitation is shown in Fig. 2(b). The input conductance is:

$$Y_{\text{in,odd}} = Y_1 \frac{Y_{\text{ino1}} + \text{j}Y_1 \tan\theta_1}{Y_1 + \text{j}Y_{\text{ino1}} \tan\theta_1} \tag{6}$$

$$Y_{\text{inoa}} = Y_2 \frac{Y_{\text{inob}} + \text{j}Y_1 \tan\theta_2}{Y_2 + \text{j}Y_{\text{inob}} \tan\theta_2} \tag{7}$$

$$Y_{\text{inob}} = -\text{j}Y_3 \cot\theta_3 \tag{8}$$

In the resonance condition ordered $Y_{\text{in,even}} = Y_{\text{in,odd}} = 0$ then there is:

$$A\left(C + \text{j}\tan\theta_3\right) - BY_3\left(1 + \text{j}C\tan\theta_3\right) = 0(\text{even-mode frequency}) \tag{9}$$

$$A + BY_3 \cot\theta_3 = 0\,(\text{Odd-mode frequency}) \tag{10}$$

$$A = R_Z Y_1^2 \left(\tan\theta_1 + R_Z \tan\theta_2\right) \tag{11}$$

$$B = \left(\tan\theta_1 \tan\theta_2 - R_Z\right) Y_1 \tag{12}$$

$$C = \frac{Y_3}{Y_{\text{ine3}}} \tag{13}$$

A detailed analysis of the governing equations reveals that, in the odd-mode state, the open-circuit stubs significantly influence the resonant frequency, while the notched circular impedance branches exhibit no effect, effectively decoupling their impact. In contrast, the even-mode resonant frequency is primarily determined by the overall MMR structure.

The resonant frequency range can be tuned by adjusting key design parameters of the resonator, including the dimensions of open-circuit stubs, electrical length (θ), and the impedance of the branches. This tunability provides flexibility for optimizing the MMR to meet specific performance requirements, such as broader bandwidth or targeted frequency responses, making it suitable for UWB filter applications.

The analyzed resonator is integrated with input and output feeders, and its overall configuration is illustrated in Fig. 3. The structure closely resembles a T-shaped resonator, with a orbicular groove introduced at the top end to enhance its performance. The grey-shaded region represents the DGS, which facilitates stronger electromagnetic coupling between the input and output ports. This enhanced coupling contributes to achieving a broader operational bandwidth.

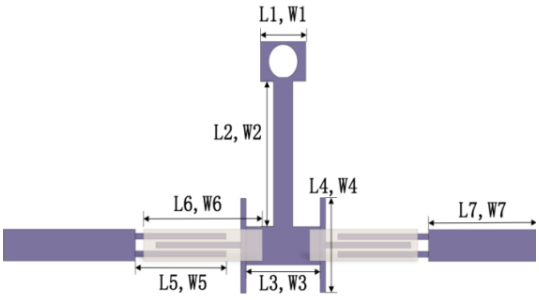

FIGURE 3. UWB filter structure.

The T-shaped resonator is strongly coupled to the parallel coupled lines at both ends, with further structural modifications applied to its top section through slotting and punching. By comparing the weak coupling and strong coupling simulations, with and without the top modifications, the results (as shown in Fig. 4) demonstrate significant improvements in the filter's performance. Specifically, the simulation results reveal that the

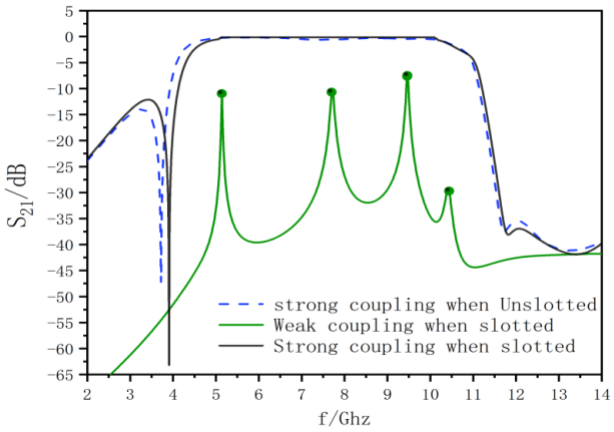

FIGURE 4. Comparison of parameters of UWB filter S_{21}.

S_{21} parameter exhibits a smoother response within the passband, and the transmission zeros in the upper and lower stopbands are attenuated by 13 dB and 5 dB, respectively, compared to the unprocessed filter.

These findings indicate that the top-end modifications effectively enhance the filter's frequency response characteristics by improving the passband performance and reducing stopband transmission zeros. Consequently, this structural optimization contributes to improved filter performance in both the passband and stopband, making it more suitable for high-performance filtering applications.

The optimized UWB filter's S-parameter characteristics are illustrated in Fig. 5. The filter achieves an upper stopband transmission zero at -58 dB and a lower stopband transmission zero at -43 dB, demonstrating an excellent out-of-band rejection level. The passband spans a frequency range from 4.5 GHz to 11 GHz, with a minimum insertion loss of 0.4 dB, and exhibits a flat response with minimal amplitude fluctuation across the passband.

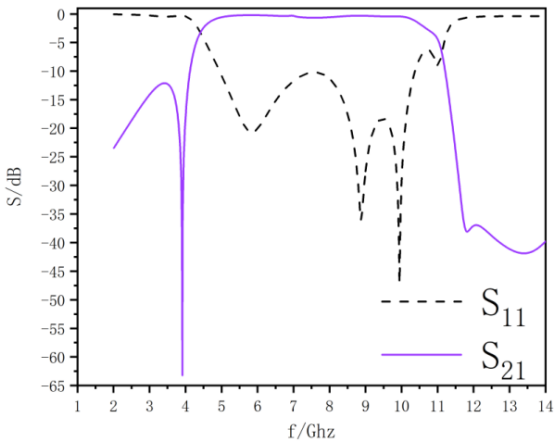

FIGURE 5. UWB filter S-parameters.

The filter's structural parameters were further optimized and fine-tuned using HFSS simulation software to achieve the desired performance metrics. The final optimized parameters are summarized in Table 1, providing a clear reference to the filter's geometric and electrical design.

TABLE 1. UWB filter dimensions.

$W1$	2.5 mm	$W5$	0.35 mm	$L4$	7.96 mm
$L1$	2.7 mm	$L5$	7.5 mm	$W4$	0.2 mm
$W2$	1.4 mm	$W6$	1.4 mm	$W7$	1.3 mm
$L2$	10.8 mm	$L6$	8.77 mm	$L7$	4.6 mm
$W3$	1.15 mm	$L3$	7.5 mm	$R1$	1.2 mm

3. DESIGN OF UWB FILTERS WITH TRAP CHARACTERISTICS

UWB filters span a broad frequency range, often overlapping with narrowband systems, which can lead to signal interference. To address this, trap structures are introduced to suppress unwanted signals while ensuring compact and efficient designs. Simultaneously, the miniaturization of filter structures remains a key objective [15].

Common methods for generating traps include using asymmetric coupled lines, additional coupled resonators, and defected ground structures (DGS) [16]. In this work, two traps are implemented using an asymmetrically coupled line and a pair of ram's horn-shaped resonators positioned beneath the input and output ports. This design achieves the effective suppression of interference, compactness, and miniaturization. The filter structure is shown in Fig. 6.

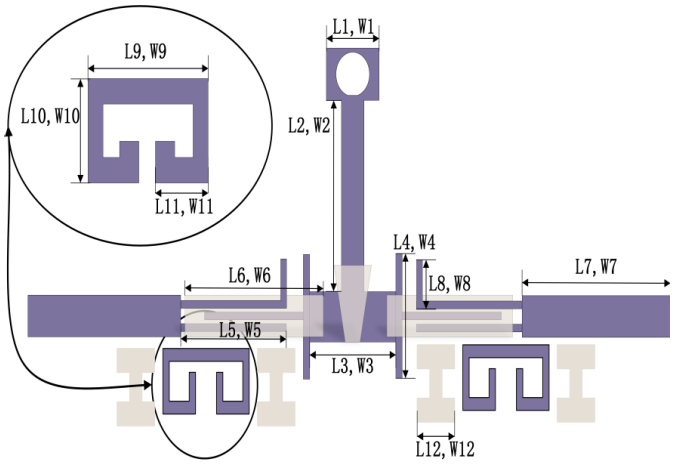

FIGURE 6. Structure of UWB filter with trap characteristic.

The first trap in this study employs an asymmetric coupling structure, formed by bending the input-output coupling line upward into an 'L'-shaped configuration, with the bending length denoted as $L8$ which is optimally adjusted to achieve the desired trapping effect, as shown in the simulation results in Fig. 7. The simulations reveal that as $L8$ increases, the center frequency of the trap gradually shifts to the left, while the trap depth is improved. However, the steepness coefficient of the trap decreases with increasing $L8$, indicating a trade-off between frequency positioning and sharpness of the trap.

When $L8 = 2.5$ mm, the trap achieves its steepest attenuation, and the center frequency is optimized at 6.8 GHz. Surface current density analysis shows that the current is concentrated

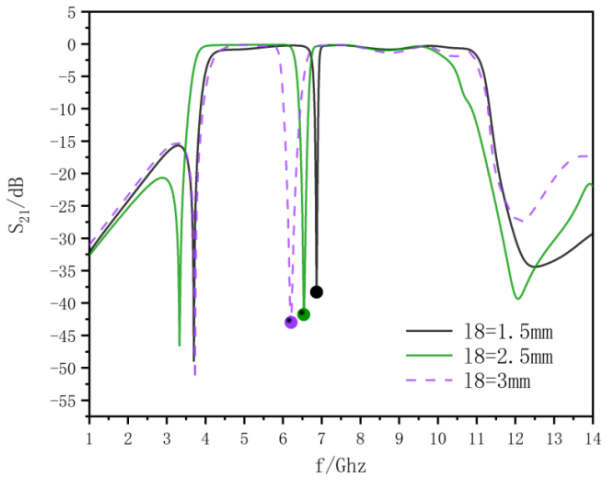

FIGURE 7. Effect of $L8$ on S_{21}.

in the asymmetric branches, effectively blocking signal transmission. This design achieves a strong trapping effect, providing effective suppression in the frequency band of meteorological satellite-related signals.

The second trapping effect is realized by introducing a pair of ram's horn-shaped resonators, whose structural configuration and parameters are detailed in the left enlargement of Fig. 6. These resonators are coupled beneath the input and output feeders to block signal transmission within a specific frequency band, thereby achieving the desired trapping effect. The resonant frequency of the ram's horn-shaped resonator is governed by the following equation [13]:

$$f_m = \frac{c}{2\left(L_9 + L_{10} + L_{11}\right)\sqrt{\varepsilon_{eff}}} \tag{14}$$

From the above equation, it is evident that the resonant frequency of the resonator is inversely proportional to its length and the relative permittivity of the dielectric material. To intuitively illustrate the effect of the resonator length on the trap frequency, simulations were conducted using HFSS software for different values of $L9$. The corresponding simulation results are presented in Fig. 8.

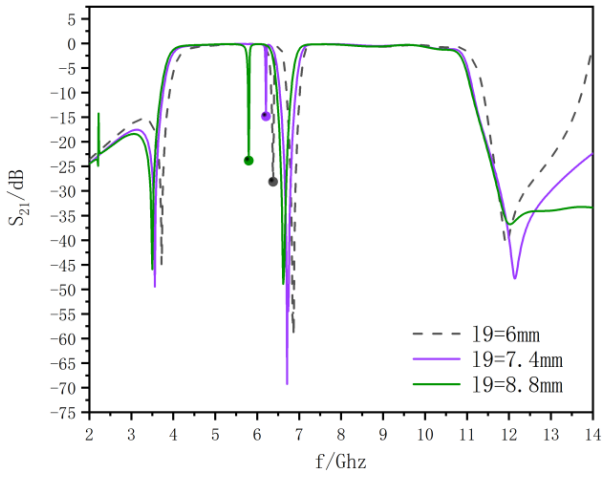

FIGURE 8. Effect of $L9$ on S_{21}.

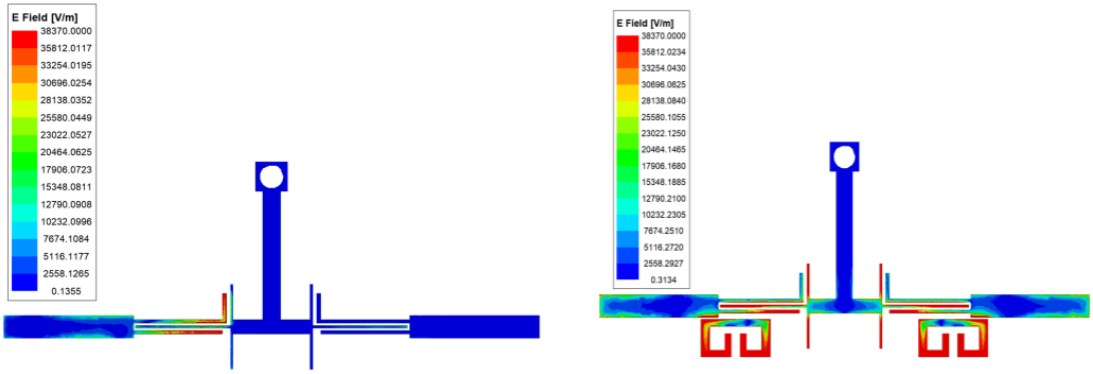

FIGURE 9. Current density transmission diagram.

The simulation results clearly show that as the length of $L9$ increases, the center frequency of the trap shifts toward the lower frequency range, while the trap position at 6.8 GHz remains unaffected. This demonstrates that the filter's trap frequency can be tuned by adjusting the length of $L9$. To mitigate the interference from certain countries operating in the Wi-Fi 6E band, the length of $L9$ is set to 7.4 mm, resulting in a trap center frequency of 6.3 GHz and a trap depth of -28.5 dB.

Figure 9 illustrates the surface current density distributions at 6.3 GHz and 6.8 GHz, respectively. As depicted, the current density is predominantly concentrated along the asymmetric coupling line and the 'ram's horn' resonator structure. This concentration of current forms effective transmission zeros which significantly attenuate signal propagation at these specific frequencies. The asymmetric coupling mechanism and the unique geometry of the 'ram's horn' resonator synergistically create high-impedance regions, thereby suppressing undesired signal transmission and enhancing the filter's selectivity in the designated stopband.

The concept of DGS was first introduced by a Korean researcher in 1999 [17]. By etching specific patterns onto the ground plane of a filter, the surface current distribution is altered, thereby affecting the transmission characteristics of the transmission line. From an equivalent circuit perspective, the DGS can be modeled as a distributed LC resonant network. The defect structures introduce additional series inductance and parallel capacitance, effectively increasing the overall inductance and capacitance per unit length of the transmission line. This enhanced LC distribution causes a reduction in the wave propagation speed, thereby increasing the phase delay and shortening the effective wavelength of the signal within the DGS region. In this study, the filter's performance is enhanced by incorporating a pair of dumbbell-shaped DGS at both ends of each ram's horn-shaped resonator and an irregular DGS directly beneath the T-shaped resonator. The detailed structure of the proposed design is illustrated in Fig. 6.

From the comparison of the S_{21} in Fig. 10, it is evident that the introduction of the Defected Ground Structure (DGS) improves the filter's performance while maintaining the original trap center frequency and trap depth. Specifically, the passband performance is enhanced, with the insertion loss in the second passband reduced by 0.2 dB and the transmission zero of the upper stopband further deepened.

As shown in the S_{11} of Fig. 10, the introduction of the DGS alters the reference ground characteristics. This change, combined with the slow-wave effect induced by the DGS, extends the electromagnetic wave's propagation time, effectively reducing reflected waves. Consequently, the return loss in the second passband is improved to less than -10 dB, meeting industrial standard requirements. These results demonstrate that the incorporation of the DGS significantly enhances the filter's performance, optimizing both passband and stopband characteristics.

4. SIMULATION AND IMPLEMENTATION

Based on the above analysis and considering the locations of the two trap center frequencies, steepness drop coefficient, and trap depths, the final structural parameters of the resonator and DGS were determined through continuous optimization. The optimized parameters are summarized in Table 2.

TABLE 2. Dimensional parameters of resonator structure.

$W9$	0.8 mm	$W10$	3.2 mm	$W11$	0.6 mm	$W12$	1 mm
$L9$	7.4 mm	$L10$	0.8 mm	$L11$	2.8 mm	$L12$	2 mm

Based on the structural parameters listed in Tables 1 and 2, a dielectric substrate of Rogers RT/duroid 5880 with a relative dielectric constant (ε_r) of 2.2 and a thickness of 0.635 mm was used to fabricate the prototype through precision machining. The fabricated prototype is shown in Fig. 11. Performance testing and analysis were conducted using a vector network analyzer, with the results also presented in Fig. 11. The measured results align closely with the simulated ones, with minor discrepancies attributed to machining tolerances and the precision limitations of the measurement equipment.

As depicted in the accompanying Fig. 11, the filter exhibits a passband ranging from 3.4 GHz to 11.8 GHz, with a minimum insertion loss of -0.2 dB and a return loss below -10 dB. The out-of-band transmission zeros are measured at -48 dB and -42 dB on the lower and upper stopbands, respectively, indicating excellent out-of-band rejection levels. Within the passband, two notch filters are implemented: the first at 6.3 GHz with a notch depth of -28.4 dB, effectively mitigating inter-

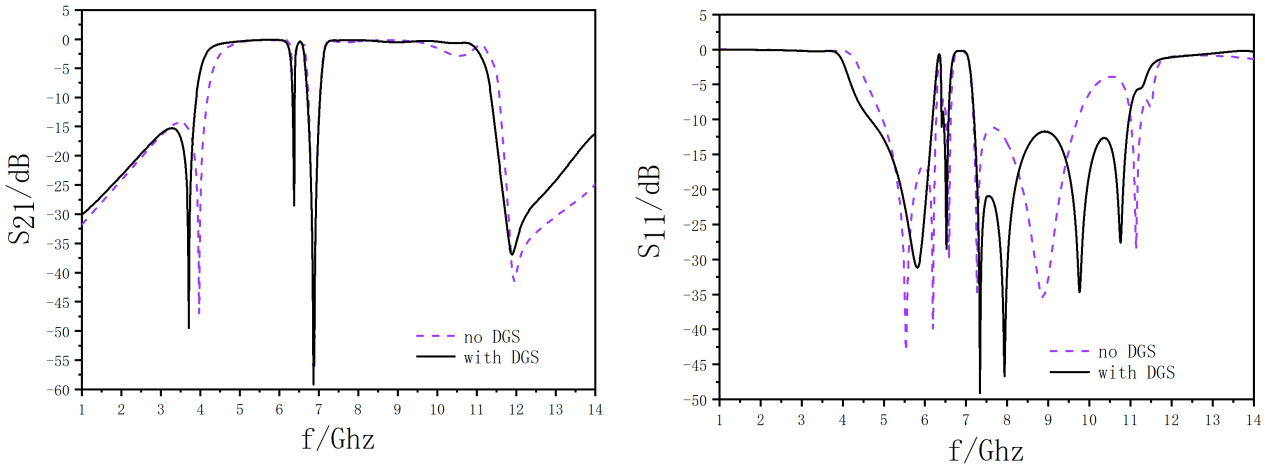

FIGURE 10. Effect of DGS on S.

TABLE 3. Filter performance comparison.

Ref.	IL/dB	RL/dB	Passband/Ghz	Attenuation at TZs/dB	Size
[7]	< 3	> 10	$2.7 \sim 11$	NA	0.3×0.16
[8]	< 0.5	> 20	$2.9 \sim 12.2$	-20	0.3×0.6
[9]	< 0.5	> 10.4	$3.0 \sim 11.5$	-19	0.5×0.118
[10]	< 0.87	$> 11,73$	$3.05 \sim 11.5$	$-22/-23.4$	0.32×0.16
[11]	< 1.84	> 10	$2.9 \sim 10.3$	$-30/-40$	0.7×1.58
[12]	< 1.13	> 10	$2.13 \sim 11.78$	$-43/-49$	0.64×0.58
this	< 0.4	> 10	$4.1 \sim 10.7$	$-28.4/-50$	0.6×0.9

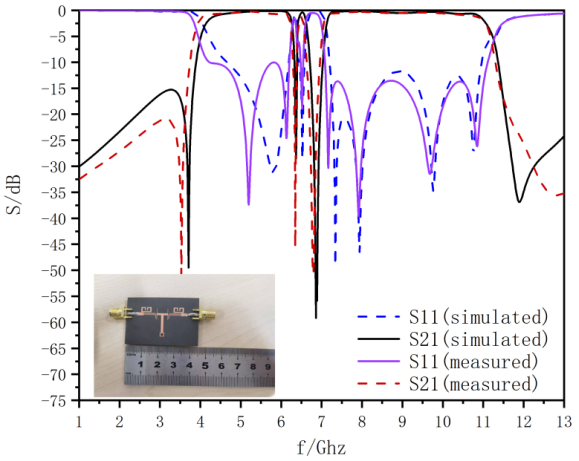

FIGURE 11. Comparison between test results and simulation results.

ference from the Wi-Fi 6E band, the second at 6.8 GHz with a notch depth of -50 dB, suppressing interference from meteorological satellite signals.

The performance parameters of the filter proposed in this study are compared with those reported in the literature [7–12], and the comparison results are summarized in Table 3. As shown, the proposed filter exhibits superior passband performance and achieves a deeper trap depth, demonstrating its advantages over previously reported designs.

5. CONCLUSION

In this study, a novel T-shaped resonator was developed by employing advanced slotting techniques to modify the traditional T-shaped resonator. The resonator was coupled with parallel coupled transmission lines at the input and output ports to design a UWB bandpass filter. Two notch bands were introduced at 6.3 GHz and 6.8 GHz by utilizing an asymmetric coupling line technique and incorporating an additional coupling structure. Furthermore, the integration of a defected ground structure (DGS) significantly enhanced the return loss performance of the filter.

The design was verified through electromagnetic simulations performed using HFSS software, and the fabricated prototype was subjected to vector network analysis for experimental validation. The results demonstrated that the proposed filter exhibits excellent out-of-band rejection characteristics while ensuring minimal distortion of signal transmission within the passband.

ACKNOWLEDGEMENT

This work was supported by the Liaoning Provincial Applied Basic Research Program (2022JH2/101300275): 5G Millimeter-wave Array Antenna Design and Research, in part by 2023 Liaoning Provincial Education Department Basic Research Project (JYTMS20230818): Research on Multi-band

Millimeter-wave Filter for 5G Wireless Communication, in part by National Natural Science Foundation of China (61971210): Future-oriented wireless reconfigurable intelligent RF module and neural network modeling research.

REFERENCES

[1] Zaki, A. I., E. F. Badran, and S. E. El-Khamy, "Two novel space-time coding techniques designed for UWB MISO systems based on wavelet transform," *PLoS ONE*, Vol. 11, No. 12, e0167990, 2016.

[2] Federal Communications Commission, "Revision of part 15 of the commission's rules regarding ultra-wideband transmission systems," First Report and Order, FCC 02-48, Washington, DC, 2002.

[3] Alqaisy, M. A., C. Chakrabraty, J. Ali, A. R. H. Alhawari, and T. Saeidi, "Reconfigurable bandwidth and tunable dual-band bandpass filter design for Ultra-Wideband (UWB) applications," *Electromagnetics*, Vol. 36, No. 6, 366–378, 2016.

[4] Ghazali, A. N. and A. Singh, "Broadside coupled UWB filter with dual notched band and extended upper stopband," in *2014 International Conference on Devices, Circuits and Communications (ICDCCom)*, 1–5, Ranchi, India, 2014.

[5] Ghazali, A. N., M. Sazid, and S. Pal, "A miniaturized microstrip-to-CPW transition based UWB-BPF with sharp roll-off and minimum insertion loss," *Microwave and Optical Technology Letters*, Vol. 58, No. 2, 289–293, 2016.

[6] Ishida, H. and K. Araki, "A design of tunable UWB filters," in *2004 International Workshop on Ultra Wideband Systems Joint with Conference on Ultra Wideband Systems and Technologies. Joint UWBST & IWUWBS 2004 (IEEE Cat. No.04EX812)*, 424–428, Kyoto, Japan, 2004.

[7] Sangam, R. S. and R. S. Kshetrimayum, "Notched UWB filter using exponential tapered impedance line stub loaded microstrip resonator," *The Journal of Engineering*, Vol. 2018, No. 9, 768–772, 2018.

[8] El Bakali, H. E. O., H. Elftouh, A. Farkhsi, and A. Zakriti, "A compact UWB bandpass filter with WLAN band rejection using hybrid technique," *Procedia Manufacturing*, Vol. 46, 922–926, 2020.

[9] Zhang, T., F. Xiao, J. Bao, and X. Tang, "A compact UWB bandpass filter with a notched band using a multistubs loaded resonator," *International Journal of RF and Microwave Computer-Aided Engineering*, Vol. 27, No. 1, e21054, 2016.

[10] Zhu, L., S. Sun, and W. Menzel, "Ultra-wideband (UWB) bandpass filters using multiple-mode resonator," *IEEE Microwave and Wireless Components Letters*, Vol. 15, No. 11, 796–798, 2005.

[11] Udhayanan, S. and K. Shambavi, "Compact single notch UWB bandpass filter with metamaterial and SIW technique," *Progress In Electromagnetics Research Letters*, Vol. 117, 41–46, 2024.

[12] Yang, S., F. Tong, Y. Chen, H. Chen, and J. Chu, "Highly compact UWB-BPF with a wide notch-band using a rectangular ring structure and two Y-shaped open stub resonators," *AEU — International Journal of Electronics and Communications*, Vol. 161, 154556, 2023.

[13] Peng, H., Y. Luo, and J. Zhao, "Compact microstrip UWB bandpass filter with two band-notches for UWB applications," *Progress In Electromagnetics Research Letters*, Vol. 45, 25–30, 2014.

[14] Zhu, L., H. Bu, and K. Wu, "Aperture compensation technique for innovative design of ultra-broadband microstrip bandpass filter," in *2000 IEEE MTT-S International Microwave Symposium Digest (Cat. No. 00CH37017)*, Vol. 1, 315–318, Boston, MA, USA, Jun. 2000.

[15] Li, R. and L. Zhu, "Compact UWB bandpass filter using stub-loaded multiple-mode resonator," *IEEE Microwave and Wireless Components Letters*, Vol. 17, No. 1, 40–42, 2007.

[16] Chen, H. and Y.-X. Zhang, "A novel and compact UWB bandpass filter using microstrip fork-form resonators," *Progress In Electromagnetics Research*, Vol. 77, 273–280, 2007.

[17] Park, J. I., C. S. Kim, J. Kim, *et al.*, "Modeling of a photonic bandgap and its application for the low-pass filter design," in *1999 Asia Pacific Microwave Conference. APMC'99. Microwaves Enter the 21st Century. Conference Proceedings (Cat. No.99TH8473)*, Vol. 2, 331–334, Singapore, Nov. 1999.